LEP Precision Results

T. Kawamoto
ICEPP, Univ. of Tokyo, 7-3-1 Hongo,
Bunkyo-ku Tokyo, 113-0033

Precision measurements at LEP are reviewed, with main focus on the electroweak measurements and tests of the Standard Model. Constraints placed by the LEP measurements on possible new physics are also discussed.

1 Introduction

A major objective of the LEP e^+e^- collider [1] is to study the Standard Model of elementary particle interactions by copiously producing the heavy gauge bosons Z and W, and making precise measurements in a systematic manner in the clean environment of the e^+e^- collisions (figure 1).

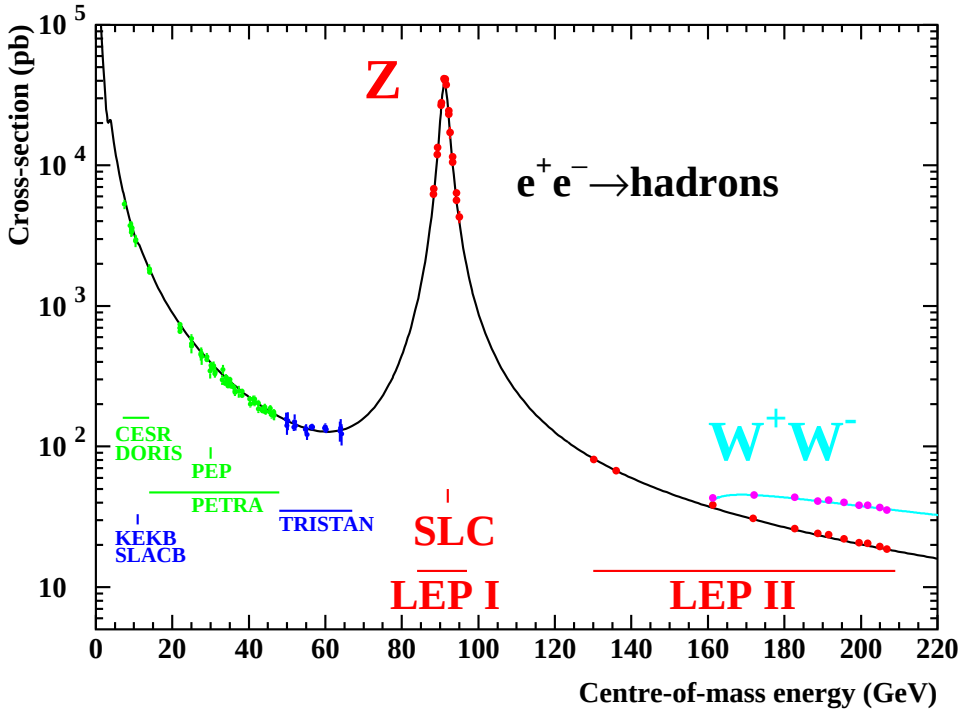

Figure 1: The hadronic cross-section in e^+e^- collision as a function of centre-of-mass energy. The solid curve is the prediction of the Standard Model, and the points are the experimental measurements.

LEP started its operation in 1989 at the centre-of-mass energy near to the Z mass. Until the

end of 1995, four LEP experiments [2], ALEPH, DELPHI, L3 and OPAL, each collected about 4.5 million Z decay events. Based on these data, the properties of the Z boson are measured with high precision allowing detailed studies of the electroweak interaction. Hadronic decays of the Z boson provides a high statistics and high purity sample of quark pair final states. Variety of QCD studies have been made. Hadronic Z decays also provide large number of b and c flavoured hadrons. Detailed studies on the properties of heavy flavours have been performed. Time dependent oscillation of B^0 and $\overline{B}^0$ was observed for the first time at LEP.

In the second phase of LEP operation (LEP2), from 1996 until 2000, centre-of-mass energy was doubled. Pair production of the W boson became possible for the first time in the e^+e^- collision, allowing precise measurements of the W boson mass and detailed studies of W pair production mechanism, which provide crucial tests of the Standard Model in different projections from those with the Z data. Measurements at LEP2 covers, as complete as possible, various final states from e^+e^- collisions at high energies. In addition to 2-fermion production which has been familiar also at lower energies, 4-fermion final states and boson pair productions are important. These allows stringent tests of the Standard Model at the new energy frontier, and provide sensitivity to various possibilities of new physics which could manifest itself as apparent deviations from the Standard Model predictions.

In this report, results of LEP precision measurements are presented and their impact to physics are discussed. Other important subjects of LEP experiment: direct searches for new particles at energy frontier, are covered in other talks in this symposium.

2 The Standard Model in brief

At tree level in the Standard Model of electroweak interaction, strength of the weak interaction, represented by the Fermi constant G_F, is related to the electromagnetic coupling α by :

$$G_F = \frac{\pi\alpha}{\sqrt{2} m_{\rm W}^2 \sin^2\theta_{\rm W}} \ , \tag{1}$$

where $m_{\rm W}$ is the W mass and $\sin^2\theta_{\rm W}$ is the electroweak mixing angle. The relation between the neutral and charged weak couplings, represented by the ρ parameter, fixes the ratio of the W and Z boson masses:

$$\rho = \frac{m_{\rm W}^2}{m_{\rm Z}^2 \cos^2\theta_{\rm W}} \ . \tag{2}$$

The ρ parameter is determined by the Higgs structure of the theory, and in the minimal Standard Model with only one Higgs doublet, ρ is unity.

The fermions (leptons and quarks) are arranged in weak iso-spin doublets for left-handed fermions, and weak iso-spin singlet for right-handed fermions.

$$\left(\begin{array}{c} \nu_\ell \\ \ell \end{array} \right)_L , \left(\begin{array}{c} \mathrm{u} \\ \mathrm{d} \end{array} \right)_L , \ell_R, \mathrm{u}_R, \mathrm{d}_R \tag{3}$$

The interaction of the Z with fermions is specified by the left- and right-handed couplings:

$$g_{\rm L} = \sqrt{\rho}(T^3 - Q\sin^2\theta_{\rm W}) \tag{4}$$

$$g_{\rm R} = -\sqrt{\rho} Q \sin^2\theta_{\rm W} \ , \tag{5}$$

Here T^3 is the third component of the weak iso-spin, and Q is the fermion charge. Alternatively vector and axial-vector couplings are:

$$g_{\rm V} = g_{\rm L} + g_{\rm R} = \sqrt{\rho}(T^3 - 2Q\sin^2\theta_{\rm W}) \tag{6}$$

$$g_{\rm A} = g_{\rm L} - g_{\rm R} = \sqrt{\rho} T^3 . \tag{7}$$

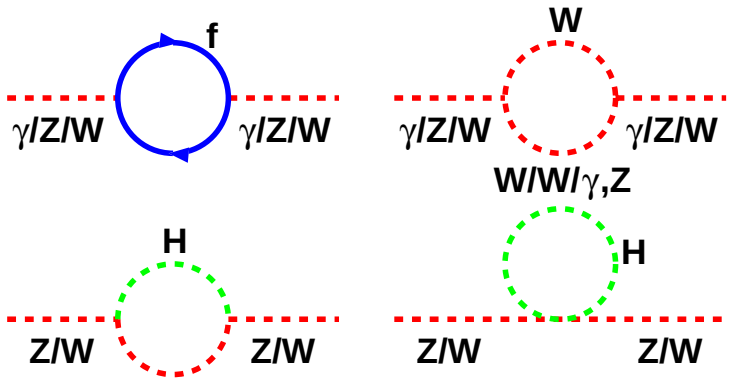

Figure 2: Higher order corrections to the gauge boson propagators due to boson and fermion loops.

These three level relations are modified by radiative corrections to the propagators as shown in figure 2. The electroweak corrections can be absorbed into the definition of the ρ parameter and the "effective" quantities:

$$\rho = 1 + \Delta\rho \tag{8}$$
$$\mathcal{S}in^2\theta_{\rm eff} = (1 + \Delta\kappa)\sin^2\theta_{\rm W} \tag{9}$$
$$\mathcal{G}_V = \sqrt{\rho}(T^3 - 2Q\mathcal{S}in^2\theta_{\rm eff}) \tag{10}$$
$$\mathcal{G}_A = \sqrt{\rho}T^3 \ . \tag{11}$$

Here $\Delta\rho$ and $\Delta\kappa$ are small complex quantities, resulting in complex effective couplings and mixing angles. In the rest of the report, the real part of these quantities are explicitly quoted, and denoted by:

$$g_V = \Re(\mathcal{G}_V), \quad g_A = \Re(\mathcal{G}_A), \quad \sin^2\theta_{\rm eff} = \Re(\mathcal{S}in^2\theta_{\rm eff}) \tag{12}$$

The correction $\Delta\rho$ and $\Delta\kappa$ have dependence on top mass $m_{\rm t}$ and Higgs mass $m_{\rm H}$. Their leading contributions, at $m_{\rm H} \gg m_{\rm W}$, are proportional to $m_{\rm t}^2$ and to much weaker $-\log(m_{\rm H})$ dependences. Flavour dependence of the radiative corrections is in general small. Only exception is for the b quark where the effects of the vertex corrections are large due to the large mass splitting between the t and b quarks, resulting in additional correction which goes as $m_{\rm t}^2$. Precise measurements of fermion-pair productions at the Z pole therefore allows access to these radiative corrections.

Relation (Eq. 1) between the coupling and $m_{\rm W}$ is also modified by the radiative corrections:

$$G_F = \frac{\pi\alpha}{\sqrt{2}m_{\rm W}^2\sin^2\theta_{\rm W}}\frac{1}{1-\Delta r} \ . \tag{13}$$

Here $\sin^2\theta_{\rm W}$, which appears also in Eq. 9, follows the on-shell definition:

$$\sin^2\theta_{\rm W} = 1 - m_{\rm W}^2/m_{\rm Z}^2 \ , \tag{14}$$

and to be distinguished from $\sin^2\theta_{\rm eff}$. The correction Δr can be divided into two components:

$$\Delta r = \Delta\alpha + \Delta r_W \tag{15}$$

The first term $\Delta\alpha$ arises from the running of the electromagnetic coupling due to fermion loops in the photon propagator. This can be divided into three contributions: leptonic loop, top quark loop and light quarks (u, d, c, s, b):

$$\Delta\alpha(s) = \Delta\alpha_\ell(s) + \Delta\alpha_{\rm top}(s) + \Delta\alpha^{(5)}_{\rm had}(s) \ . \tag{16}$$

The $\Delta\alpha_\ell(s)$ term due to leptonic loop can be calculated precisely, and the small top contribution can also be calculated adequately, whereas the hadronic term $\Delta\alpha^{(5)}_{\rm had}(s)$ is determined using data of hadronic cross-section in e^+e^- collision. Low energy e^+e^- data is particularly important. Improved measurements at $\sqrt{s}$ =2-3 GeV have recently been obtained from the BES collaboration [3]. Using these new results improved evaluations of this quantity have been made [4].

The Δr_W term contains $m_{\rm t}^2$ and $\log(m_{\rm H})$ dependent corrections. With precise measurements of $m_{\rm W}$ these electroweak corrections can be probed.

3 Measurements at the Z pole

In the e^+e^- collision at centre-of-mass energy near to the Z mass, contribution to the cross-section from s-channel resonance due to the Z boson dominates over that of the photon exchange by a factor of $\mathcal{O}(1000)$. Therefore the fermion pair final states at LEP is a very pure and clean sample of Z decays. Figure 3 illustrates typical physics topics studied at the Z pole. In this section, precision measurements of the Z properties and QCD studies are discussed.

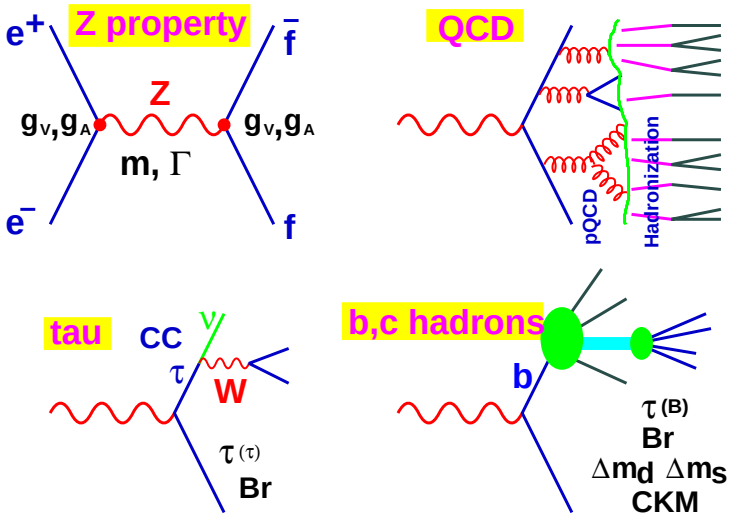

Figure 3: Physics topics at the Z pole.

3.1 Zedometry

The process $e^+e^- \to f\bar{f}$ is mediated in the s-channel by two spin-1 neutral gauge bosons, a massless photon and a massive Z boson. The cross-section can be parametrised by Breit-Wigner resonance for the Z contribution and remaining contributions from photon exchange and γ-Z interference:

$$\sigma_{\rm f}(s) = \sigma^0_{\rm f}\frac{s\Gamma_{\rm Z}^2}{(s-m_{\rm Z}^2)^2+s^2\Gamma_{\rm Z}^2/m_{\rm Z}^2} + \sigma(\gamma) + \sigma(\gamma-{\rm Z}) \tag{17}$$

with

$$\sigma^0_{\rm f} = \frac{12\pi}{m_{\rm Z}^2}\frac{\Gamma_{\rm e}\Gamma_{\rm f}}{\Gamma_{\rm Z}^2}\ , \tag{18}$$

where $\Gamma_{\rm f}$ is the partial width to fermion f. Measurement of the resonance curve, the Z lineshape, allows precise determination of the mass $m_{\rm Z}$ and the total width $\Gamma_{\rm Z}$ of the Z boson, and the peak cross-section $\sigma^0_{\rm f}$ of the resonance. By combining lineshape measurements of all visible fermion-pair final states f = e, μ, τ, hadrons(q), partial width $\Gamma_{\rm f}$ can be extracted. This conceptually

simple measurement has lead to the first physics publications from the LEP collaborations. The important result from these first LEP results, in addition to significant improvements on the determination of $m_{\rm Z}$ and $\Gamma_{\rm Z}$, is the determination of the number of neutrino species to be three for the first time with the uncertainty below ± 1.

Due to the parity violating coupling of the Z to fermions, various asymmetries arise in the process $\rm e^+e^- \to Z \to f\bar{f}$. This can be seen by writing down cross-sections for different helicity combinations:

$$\sigma_{LL}(\cos\theta) = C(s) \cdot g^2_{L\rm e} g^2_{L\rm f} (1+\cos\theta)^2 \quad (19)$$

$$\sigma_{LR}(\cos\theta) = C(s) \cdot g^2_{L\rm e} g^2_{R\rm f} (1-\cos\theta)^2 \quad (20)$$

$$\sigma_{RL}(\cos\theta) = C(s) \cdot g^2_{R\rm e} g^2_{L\rm f} (1-\cos\theta)^2 \quad (21)$$

$$\sigma_{RR}(\cos\theta) = C(s) \cdot g^2_{R\rm e} g^2_{R\rm f} (1+\cos\theta)^2 \quad (22)$$

where $C(s)$ is the centre-of-mass energy dependent common coefficient, and $\sigma_{ij}(i,j = L,R)$ are differential cross-section for the process $\rm e^+e^- \to Z \to f\bar{f}$ with left(L)- or right(R)-handed initial-state electron and left- or right-handed final-state fermion f. Left- and right-handed couplings are denoted by g_i, and in the Standard Model they are as defined in Eq. 4 and 5.

- Angular distribution for unpolarised beams, ignoring the final-state helicity.
  Cross-section is obtained by averaging over initial-state helicity and summing over final-state helicity.

$$\begin{aligned} \sigma(\cos\theta) &= \frac{1}{2}(\sigma_{LL} + \sigma_{LR} + \sigma_{RL} + \sigma_{RR}) \\ &\propto (g^2_{V\rm e} + g^2_{A\rm e})(g^2_{V\rm f} + g^2_{A\rm f}) \cdot (1 + \cos^2\theta + 2\mathcal{A}_{\rm e}\mathcal{A}_{\rm f}\cos\theta), \end{aligned} \quad (23)$$

  where the asymmetry parameter $\mathcal{A}_{\rm f}$ is defined by:

$$\mathcal{A}_{\rm f} = \frac{2 g_{V\rm f} g_{A\rm f}}{g^2_{V\rm f} + g^2_{A\rm f}} \ . \quad (24)$$

  Forward-backward asymmetry $A_{\rm FB} = (\sigma_{\rm F} - \sigma_{\rm B})/(\sigma_{\rm F} + \sigma_{\rm B})$ arise from the term proportional to $\cos\theta$, and is given by:

$$A_{\rm FB} = \frac{3}{4}\mathcal{A}_{\rm e}\mathcal{A}_{\rm f} \quad (25)$$

- Polarisation of final-state fermion, unpolarised beams.
  In the τ-pair final-state, polarisation of taus can be measured based on the V-A charged current decays of taus. The tau polarisation $\mathcal{P}_\tau(\cos\theta) = (\sigma_R - \sigma_L)/(\sigma_R + \sigma_L)$ is given by:

$$\mathcal{P}_\tau(\cos\theta) = \frac{(\sigma_{LR} + \sigma_{RR}) - (\sigma_{LL} + \sigma_{RL})}{(\sigma_{LR} + \sigma_{RR}) + (\sigma_{LL} + \sigma_{RL})} \quad (26)$$

$$= \frac{\mathcal{A}_\tau(1 + \cos^2\theta) + 2\mathcal{A}_{\rm e}\cos\theta}{(1 + \cos^2\theta) + 2\mathcal{A}_{\rm e}\mathcal{A}_\tau\cos\theta} \quad (27)$$

  The forward-backward symmetric term is proportional to $\mathcal{A}_\tau$, while the anti-symmetric term is proportional to $\mathcal{A}_{\rm e}$. From the measurement of τ-polarisation, $\mathcal{A}_{\rm e}$ and $\mathcal{A}_{\rm f}$ are extracted separately.

- With polarised beam, cross-section asymmetry A_{LR}.
  Measured by the SLD experiment at the SLC collider using polarised electron beam [5]. Left-right cross-section asymmetry directly determines $\mathcal{A}_{\rm e}$.

$$A_{LR} = \frac{(\sigma_{LL} + \sigma_{LR}) - (\sigma_{RL} + \sigma_{RR})}{(\sigma_{LL} + \sigma_{LR}) + (\sigma_{RL} + \sigma_{RR})} \quad (28)$$

$$= \mathcal{A}_{\rm e} \quad (29)$$

here σ_{ij} is the cross-section integrated over $\cos\theta$ within forward-backward symmetric acceptance. Alternatively, forward-backward asymmetry of the left-right asymmetry, A_{FBLR}, gives the asymmetry parameter of the final-state fermion:

$$A_{FBLR} \;=\; \frac{3}{4}\mathcal{A}_{\rm f} \tag{30}$$

Forward-backward asymmetries are measured at LEP for charged leptons e, μ and τ, and for b and c quarks. Using the measurements of $\mathcal{A}_{\rm e}$, the parameters $\mathcal{A}_\mu$, $\mathcal{A}_\tau$, $\mathcal{A}_{\rm b}$ and $\mathcal{A}_{\rm c}$ can also be inferred from forward-backward asymmetry measurements at LEP using Equation 25. At SLC A_{LR} and A_{FBLR} measurements determined the parameters $\mathcal{A}_{\rm e}$, $\mathcal{A}_\mu$, $\mathcal{A}_\tau$, $\mathcal{A}_{\rm b}$ and $\mathcal{A}_{\rm c}$. Therefore the LEP and SLC results form a complementary and practically complete set of the $\mathcal{A}_{\rm f}$ measurements. If the couplings conform to the Standard Model relations, then effective mixing angle can be inferred from the measurements of $\mathcal{A}_{\rm f}$ through:

$$\frac{g_{V{\rm f}}}{g_{A{\rm f}}} = (1 - \frac{2Q}{T^3}\sin^2\theta^{\rm f}_{\rm eff}) \;. \tag{31}$$

Lineshape and leptonic $A_{\rm FB}$

A set of precision measurements of basic quantities, cross-sections for hadronic and leptonic final-states, and leptonic forward-backward asymmetries provide rich information on the properties of the Z, and allow important tests of the Standard Model. The mass $m_{\rm Z}$, the total width $\Gamma_{\rm Z}$ and pole cross-section $\sigma^0_{\rm f}$ are determined from the lineshape measurement, by measuring the cross-section for the process $e^+e^- \to f\bar{f}$ as a function of centre-of-mass energy around the Z resonance at $\sqrt{s} \approx m_{\rm Z}$ (figure 4). How well these parameters can be determined depends on

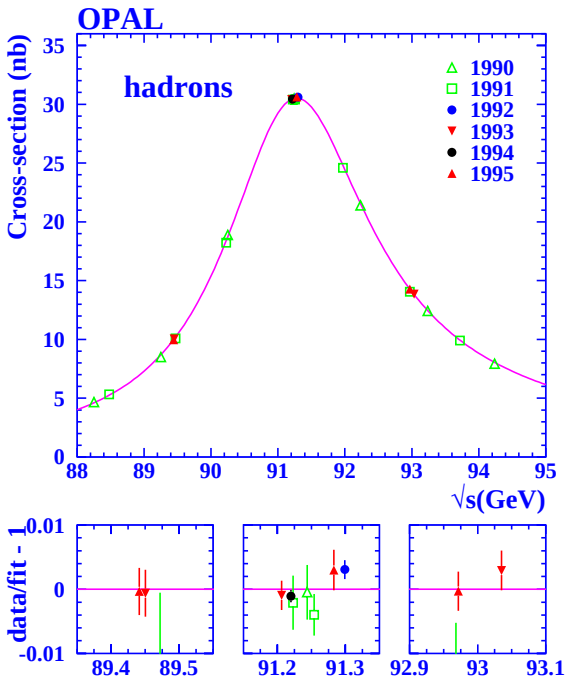

Figure 4: A measurement of Hadronic lineshape.

how accurately the "lineshape" is determined. Since the hadronic final-state is the dominant

decay mode of the Z, $m_{\rm Z}$ and $\Gamma_{\rm Z}$ are mainly determined from the hadronic lineshape. The data sample from 1993-1995 is particularly important. In this running period, precision energy scans have been performed at three centre-of-mass energy points on the peak and two off-peak points approximately 1.8 GeV above and below the peak. About 36 pb^{-1} of integrated luminosity were collected by each of the LEP experiments at the off-peak points, almost equally distributed to peak-2 and peak+2 GeV points, allowing high statistics for the determination of $m_{\rm Z}$ and $\Gamma_{\rm Z}$. In 1994 all data were collected on peak and about 55 pb^{-1} were collected. Measurements of $\sigma^0_{\rm f}$ and the pole asymmetry $A^{0,{\rm f}}_{\rm FB}$ profit from the high statistics measurements at the peak.

Systematic uncertainties must also be under control in order to make full use of the statistical precision. Key issues are:

- Event selection: evaluation of efficiency and background.
- Determination of luminosity.
- Precise calibration of LEP beam energy.
- Precision calculation of radiative correction.

All of these were studied carefully and systematic uncertainties on the cross-section and asymmetry measurements are controlled to better than 0.1% level. Successful calibration of LEP energy achieved a relative accuracy of 10^{-5} level [6]. Uncertainties on $m_{\rm Z}$ and $\Gamma_{\rm Z}$ arising from LEP energy uncertainty are $\pm$1.7 MeV and $\pm$1.2 MeV, respectively. The cross-section formula Equation 17 is largely modified due to radiative corrections, mainly by initial-state radiation. In order to interpret the precisely measured quantities, quality of theoretical calculations must match the experimental precision. Achieved theoretical precision of the calculations as implemented in the programs ZFITTER [7] and TOPAZ0 [8], is typically to the 10^{-4} level [9].

Using these data, lineshape and lepton asymmetries are analysed by fitting theoretical parameterisations to the data. The standard set of the parameters are:

- $m_{\rm Z}$ and $\Gamma_{\rm Z}$, defined in terms of Breit-Wigner denominator $s - m_{\rm Z}^2 + is\Gamma_{\rm Z}/m_{\rm Z}$.
- The hadronic pole cross-section

$$\sigma^0_{\rm had} = \frac{12\pi}{m_{\rm Z}^2}\frac{\Gamma_{\rm e}\Gamma_{\rm had}}{\Gamma_{\rm Z}^2} \tag{32}$$

- Partial width ratios:

$$R^0_\ell = \frac{\Gamma_{\rm had}}{\Gamma_\ell}, \quad \ell = {\rm e}, \mu, \tau \tag{33}$$

- Leptonic pole asymmetries, defined in terms of the real part of effective couplings.

$$A^{0,\ell}_{\rm FB} = \frac{3}{4}\mathcal{A}_{\rm e}\mathcal{A}_\ell \tag{34}$$

Results from the four LEP experiments are combined [10] to obtain best results from LEP which are summarised in figure 21. The Z mass has been determined to a relative precision of 10^{-5}, $m_{\rm Z} = 91.1875 \pm 0.0021$ GeV. Figure 5 shows in the R^0_ℓ - $A^{0,\ell}_{\rm FB}$ plane the results of leptonic widths and asymmetries. The results for three lepton species are consistent each other, supporting the universality of leptons. Partial decay widths can be derived from these parameters. The ratio of invisible width, $\Gamma_{\rm inv} = \Gamma_{\rm Z} - \Gamma_{\rm e} - \Gamma_\mu - \Gamma_\tau - \Gamma_{\rm had}$, to the leptonic width is:

$$\Gamma_{\rm inv}/\Gamma_\ell = 5.942 \pm 0.016 \ . \tag{35}$$

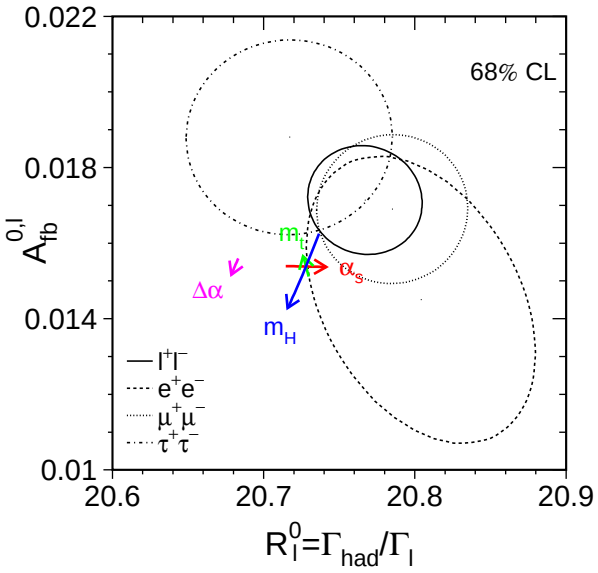

Figure 5: Contour of 68% probability in the $R_\ell^0 - A_{\rm FB}^{0,\ell}$ plane. The Standard Model prediction for $m_{\rm Z} = 91.1875$ GeV, $m_{\rm t} = 174.3 \pm 5.1$ GeV, $m_{\rm H} = 300^{+700}_{-186}$ GeV, and $\alpha_s(m_{\rm Z}) = 0.118 \pm 0.002$ is also shown.

Assuming the invisible width is due to neutrinos, and using the Standard Model expectation for this ratio a single neutrino species $(\Gamma_\nu/\Gamma_\ell)_{\rm SM} = 1.9912 \pm 0.0012$, the number of neutrino species is obtained as:

$$N_\nu = (\Gamma_{\rm inv}/\Gamma_\ell)/(\Gamma_\nu/\Gamma_\ell)_{\rm SM} = 2.9841 \pm 0.0083 \tag{36}$$

which is consistent with three. Alternatively, assuming $N_\nu = 3$ additional contribution to the invisible width is

$$\Delta\Gamma_{\rm inv} = -2.7 \pm 1.6 \ \ {\rm MeV}, \tag{37}$$

and the 95% confidence level upper limit on the additional width is

$$\Delta\Gamma_{\rm inv} < 2.0 \ \ {\rm MeV} \tag{38}$$

τ polarisation

The fermion pair produced via the Z resonance is polarised according to Eq. 19. Here the polarisation is defined as:

$$P = \frac{\sigma_R - \sigma_L}{\sigma_R + \sigma_L} \ , \tag{39}$$

where σ_R and σ_L are respectively cross-section for production of right- and left-handed fermions with unpolarised beams. In the τ-pair production, polarisation can be measured from the kinematic distributions of τ decay products. An example of a simple case for $\tau \to \pi\nu$ decay is illustrated in figure 6. Observed momentum distribution of charged π is also shown in the figure. Observed distributions are in general distorted from the original distribution due to detector effects, bias arising from event selection and radiative effects. Monte Carlo simulation is used to take into account such effects.

Distribution of the kinematic variable is a linear combination of two distributions, one corresponding to helicity h=+1 and the other to h=–1, and the relative fraction of the two contributions is determined by the τ polarisation. The LEP experiments have analysed all relevant decay modes: $\tau \to \pi\nu_\tau$, $\rho\nu_\tau$, $\mathrm{a_1}\nu_\tau$, $\mathrm{e}\nu_\tau\nu_\mathrm{e}$, $\mu\nu_\tau\nu_\mu$. Depending on the nature of each decay mode, an optimal kinematic observable is constructed and used for fitting the polarisation. Combined τ polarisation measurements are shown as a function of $\cos\theta$ in figure 7. The data behave

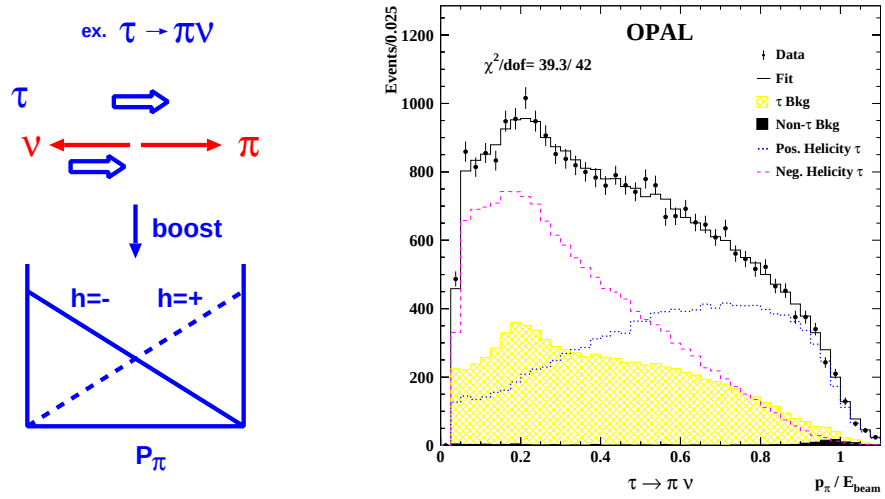

Figure 6: Left: Illustration of tau polarisation measurement. Right: Measured distribution of kinematic variable for the $\tau \to \pi\nu$ mode.

as expected from Eq. 27. Separately extracted $\mathcal{A}_{\rm e}$ and $\mathcal{A}_\tau$ from the τ polarisation measurements are summarised in figure 7. Results from the four experiments agree well, and $\mathcal{A}_{\rm e}$ and $\mathcal{A}_\tau$ are consistent with equality as expected from the lepton universality. The current result of combined leptonic asymmetry parameter $\mathcal{A}_\ell$ from the τ polarisation measurements is [11] $\mathcal{A}_\ell = 0.1465 \pm 0.0033$.

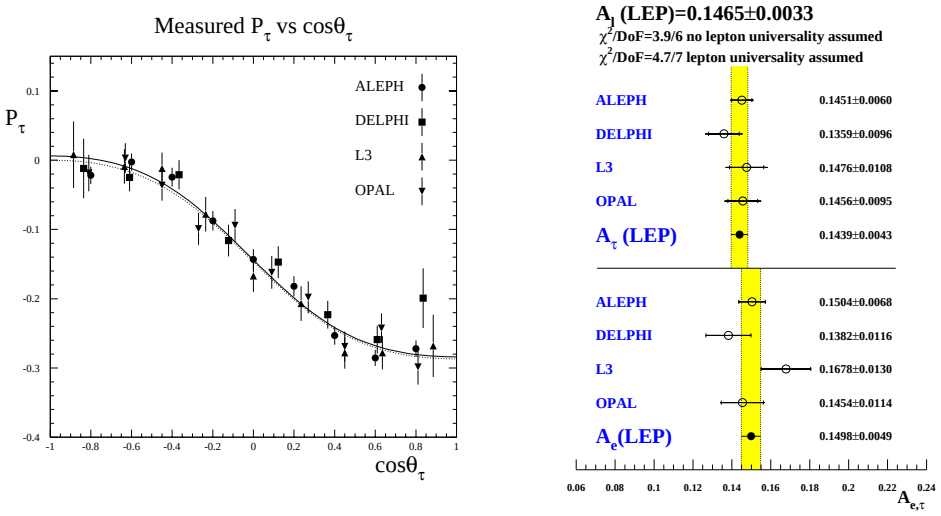

Figure 7: Left: P_τ as a function of $\cos\theta$. The curves are expectation from Eq. 27 with and without assuming equality of $\mathcal{A}_{\rm e}$ and $\mathcal{A}_\tau$. Right: Results of $\mathcal{A}_{\rm e}$ and $\mathcal{A}_\tau$ measurements.

b and c widths and $A_{\rm FB}$

Z decays into b and c quarks can be identified with good purity allowing measurements of production rates and forward-backward asymmetries for b and c quarks. From the tagged b and c samples, information on the Z partial widths into b and c quarks, and forward-backward asymmetries are extracted.

- Ratios of b and c partial width to the hadronic width:

$$R_{\rm b}^0 = \Gamma_{\rm b}/\Gamma_{\rm had}, \quad R_{\rm c}^0 = \Gamma_{\rm c}/\Gamma_{\rm had} \tag{40}$$

- forward-backward pole asymmetries:

$$A_{\rm FB}^{0,{\rm b}} = \frac{3}{4}\mathcal{A}_{\rm e}\mathcal{A}_{\rm b}, \quad A_{\rm FB}^{0,{\rm c}} = \frac{3}{4}\mathcal{A}_{\rm e}\mathcal{A}_{\rm c} \tag{41}$$

At SLC, using the polarised electron beam, the SLD experiment measured, in addition to $R_{\rm b}^0$ and $R_{\rm c}^0$, the b and c quark asymmetry parameters from A_{FBLR}:

- from forward-backward left-right asymmetry A_{FBLR}:

$$\mathcal{A}_{\rm b}, \quad \mathcal{A}_{\rm c} \tag{42}$$

Various tagging techniques are developed. The lepton tag is based on the weak semi-leptonic decays of b/c flavoured hadrons. Due to the large mass of b/c hadrons, these leptons tend to have high momentum (p), and transverse momentum (p_t) with respect to the jet axis also tends to be large. Separation between b and c quarks is made based on different (p, p_t) spectra for b$\to\ \ell$, b$\to$c$\to\ \ell$ and c$\to\ \ell$. For the asymmetry measurements, charge of the lepton provide information to distinguish q from $\bar{\rm q}$. Powerful method of b tagging is based on the long life time (typically 1.5 ps) and large mean charged multiplicity of B hadron decays. The LEP detectors were equipped with precision vertex detectors [1] which allow detecting signatures of displaced decay vertex, either by directly reconstructing the secondary vertex, or based on a large number of tracks with significant impact parameter. Large invariant mass of the particles from the secondary vertex is also an indication of B hadron decays. Other useful information is from the event shape of b jets being different from that of light quarks. These sensitive variables are often combined using artificial neural network or likelihood technique. Figure 8 shows a few example of such b-tagging variables.

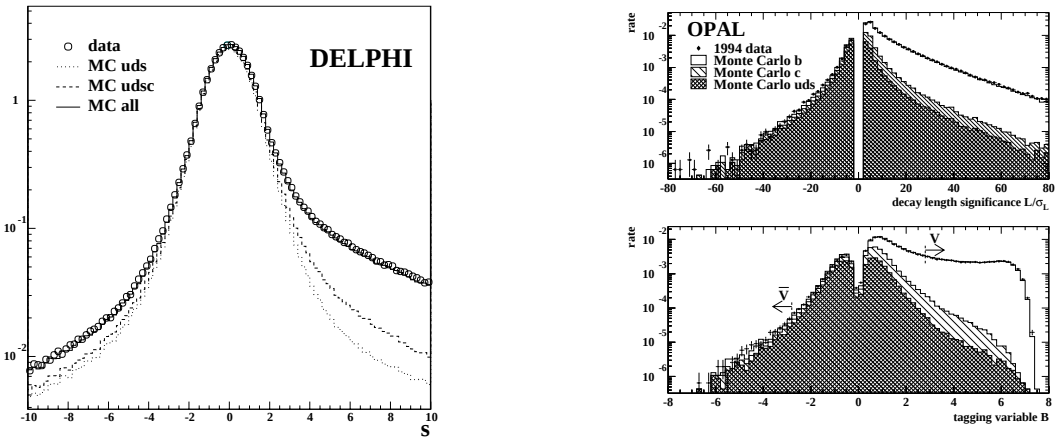

Figure 8: Examples of b-tagging variables.

Results of $R_{\rm b}^0$ and $A_{\rm FB}^{0,{\rm b}}$ from LEP experiments and SLD are summarised in figure 9. Results from different experiments and from different techniques are consistent. Combination [12] has been made using these measurements to produce a set of b and c quark measurements on $R_{\rm b}^0$, $R_{\rm c}^0$, $A_{\rm FB}^{0,{\rm b}}$, $A_{\rm FB}^{0,{\rm c}}$, $\mathcal{A}_{\rm b}$ and $\mathcal{A}_{\rm c}$. In the b/c measurements, the SLD experiment profited from the small beam size and small beam pipe of the SLC collider which enabled tagging b quarks with higher efficiency than LEP experiments. This allowed SLD to perform competitive measurements $R_{\rm b}^0$ and $R_{\rm c}^0$ despite much lower statistics of the Z sample ($\approx 1/10$ of LEP).

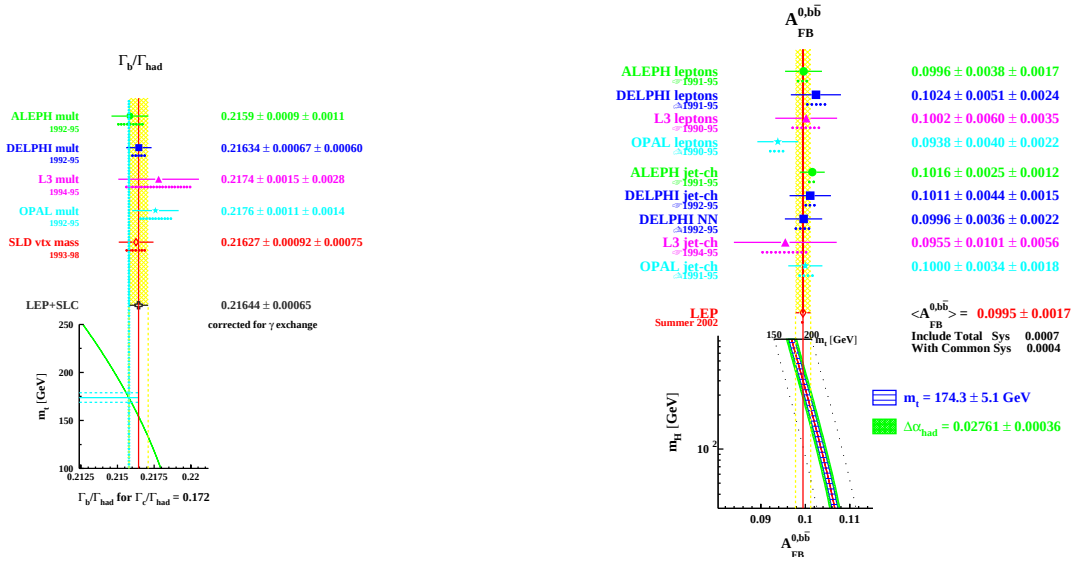

Figure 9: Results of R_b^0 and $A_{FB}^{0,b}$ measurements.

Z couplings

Results of the asymmetry parameter $\mathcal{A}_f$ are summarised graphically in figure 10. Leptonic asymmetry $\mathcal{A}_\ell$ is obtained from combination of leptonic forward-backward asymmetries, τ polarisation and the A_{LR} measurements, assuming lepton universality. For b quark, $\mathcal{A}_b$ is from the SLD A_{FBLR} measurement. These two measurements are presented in the figure by vertical and horizontal bands. Forward-backward asymmetry for b quark, $A_{FB}^{0,b}$, is a product of $\mathcal{A}_\ell$ and $\mathcal{A}_b$, therefore represented by the diagonal band in the $\mathcal{A}_\ell$ - $\mathcal{A}_b$ plane. The three bands agree

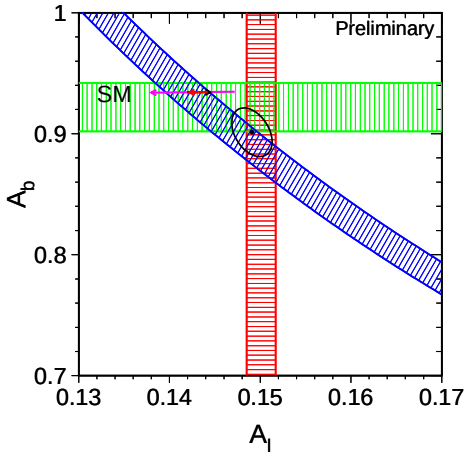

Figure 10: The measurements of combined LEP+SLD $\mathcal{A}_\ell$, SLD $\mathcal{A}_b$, and LEP $A_{FB}^{0,b}$, compared to the Standard Model expectations (arrows). Also shown is a 68% probability contour from a joint analysis.

reasonably well, having a common value in the plane as indicated by the 68% confidence level contour. However the combined value [12] of $\mathcal{A}_b = 0.901 \pm 0.013$ is 2.6 standard deviation away from the Standard Model expectation of 0.935. This is mainly because the intersect of $A_{FB}^{0,b}$ and $\mathcal{A}_\ell$ bands deviates largely from the Standard Model value. In the Standard Model, as seen in

the figure, $\mathcal{A}_{\rm b}$ is rather stable quantity insensitive to any of the Standard Model parameters. The large deviation of the combined contour may be simply due to fluctuation of one or both of the $A_{\rm FB}^{0,{\rm b}}$ and $\mathcal{A}_\ell$ measurements, or could be arising from some new physics which involves non-standard b couplings. Direct determination of $\mathcal{A}_{\rm b}$ is not precise enough to distinguish the two possibilities.

From the asymmetries $\mathcal{A}_{\rm f}$ and partial decay widths $\Gamma_{\rm f}$, vector and axial-vector couplings can be extracted; $\mathcal{A}_{\rm f}$ determines $(g_{V{\rm f}}/g_{A{\rm f}})$, while $\Gamma_{\rm f}$ determines $(g_{V{\rm f}}^2+g_{A{\rm f}}^2)$. Results for lepton, b and c couplings obtained from LEP and SLD partial widths and asymmetry measurements are shown figure 11. Results for three lepton species agree well as expected from the lepton universality.

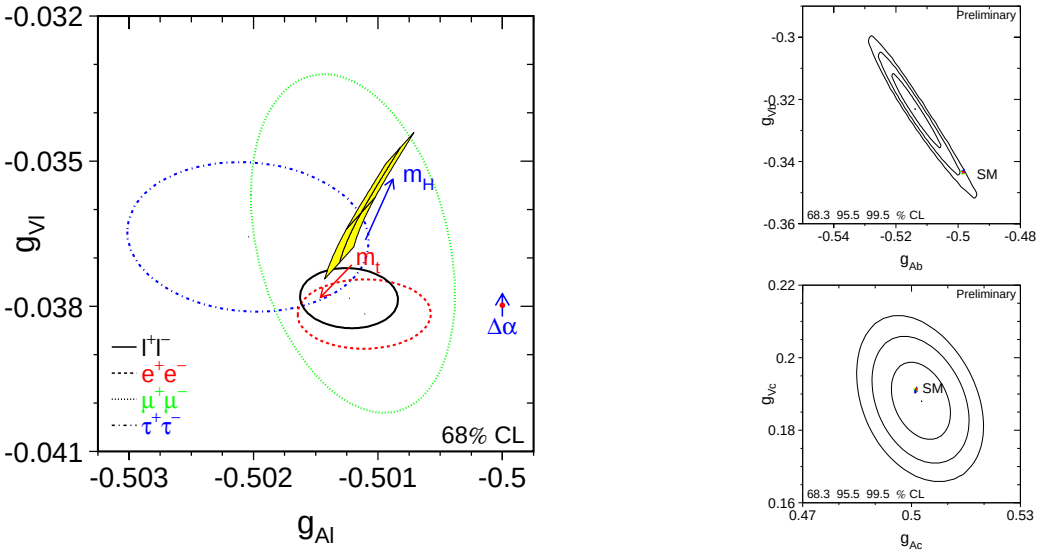

Figure 11: Contours in the $g_{V{\rm f}}$-$g_{A{\rm f}}$ plane for leptons, b and c quark.

The combined result assuming lepton universality is also shown in the plot. The vertical arrow $(\Delta\alpha)$ shows the expectation where only the running of α is considered $(g_{A\ell} = -1/2)$. The observed value of $g_{A\ell}$ is significantly different from this expectation, which demonstrate the effect of electroweak correction $\Delta\rho$. Also shown is the expectation of the Standard Model. The result of lepton couplings prefers low Higgs mass. The b coupling is not quite consistent with the Standard Model, as already seen in the $\mathcal{A}_\ell$ - $\mathcal{A}_{\rm b}$ plot. As the determination of $\mathcal{A}_{\rm b}$ relies largely on $A_{\rm FB}^{0,{\rm b}}$ and $\mathcal{A}_\ell$ via $\mathcal{A}_{\rm b} = (4/3)A_{\rm FB}^{0,{\rm b}}/\mathcal{A}_\ell$, fluctuation of either of $A_{\rm FB}^{0,{\rm b}}$ or $\mathcal{A}_\ell$ can cause the shift of combined $\mathcal{A}_{\rm b}$.

If the Z couplings follow the Standard Model structure, the ratio of vector and axial-vector couplings $g_{V{\rm f}}/g_{A{\rm f}}$ can be represented by the effective mixing angle $\sin^2\theta_{\rm eff}^{\rm f}$ as given by Eq. 31. Asymmetry measurements are used to extract effective mixing angle. As already seen above in figure 10, $\mathcal{A}_{\rm b}$ and $\mathcal{A}_{\rm c}$ are insensitive to the Standard Model parameters, thus insensitive to the value of $\sin^2\theta_{\rm eff}^{\rm q}$. This can be seen in figure 12 where dependence of $\mathcal{A}_{\rm f}$ on $\sin^2\theta_{\rm eff}^{\rm f}$ is shown for lepton, b and c quark. Therefore $A_{\rm FB}^{0,{\rm b}}$ can be used to determine $\mathcal{A}_\ell$ via $\mathcal{A}_\ell = (4/3)A_{\rm FB}^{0,{\rm b}}/\mathcal{A}_{\rm b}$ with $\mathcal{A}_{\rm b}$ constrained to the Standard Model expectation (as a function of $\sin^2\theta_{\rm eff}^{\rm lept}$). Effective mixing angle for lepton, $\sin^2\theta_{\rm eff}^{\rm lept}$, determined from $\mathcal{A}_\ell$ measurements from different processes are summarised in figure 12. Two most precise determinations, one from A_{LR} by SLD and the other from $A_{\rm FB}^{0,{\rm b}}$ at LEP, differ by 2.9 standard deviation. This difference is reflected in the overall χ^2 of the average; $\chi^2/{\rm d.o.f} = 10.2/5$, corresponding to a probability of 7.0%. The origin of this difference is as already seen in the comparison of $\mathcal{A}_{\rm f}$ in the discussion of asymmetries. If there were some new physics contribution that affect the b coupling to largely deviate from the Standard Model, the extraction of $\sin^2\theta_{\rm eff}^{\rm lept}$ from the $A_{\rm FB}^{0,{\rm b}}$ does not work.

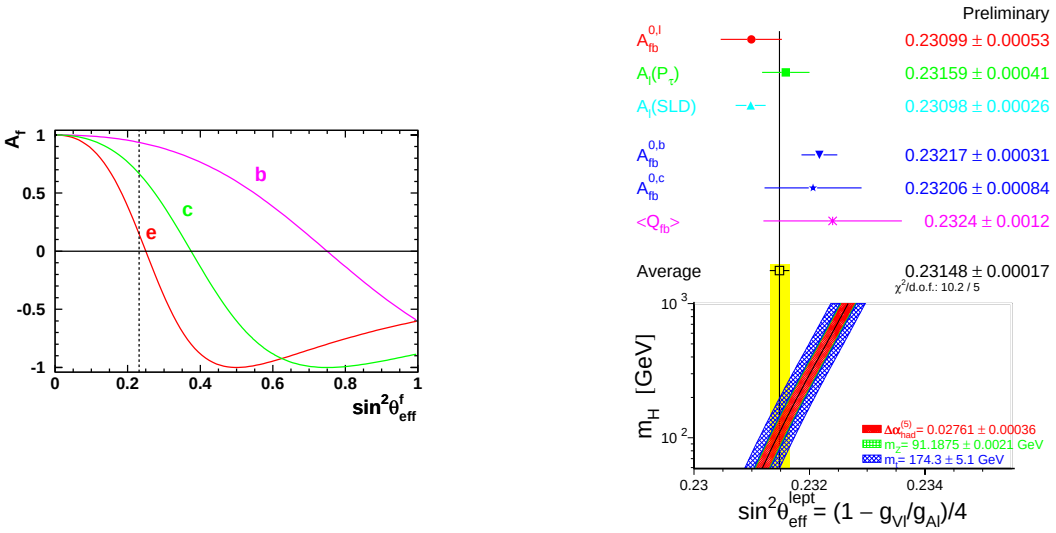

Figure 12: Left: Dependence of $\mathcal{A}_f$ on $\sin^2\theta^f_{eff}$ for lepton, b and c quark. Right: Comparison of determinations of $\sin^2\theta^{lept}_{eff}$ from asymmetry measurements. Also shown is the prediction of the Standard Model as a function of Higgs mass.

3.2 QCD studies

A large number of quark-pair final states from Z decays provides a clean high purity sample for QCD studies, both for perturbative QCD at high energy scale ($\sqrt{s}$), hadronisation at low energy scale ($\mathcal{O}$(100 MeV)), and physics of hadrons (figure 3). At LEP2 energies statistics of hadronic sample is much lower compared to at the Z pole. Purity of quark-pair sample is also lower, mainly due to background from W pair events and complication due to the radiative Z return (see Section 4.1). However, measurements at LEP2 allows to study the energy evolution of QCD over wide range of energy. Two topics out of a large variety of QCD studies [13] at LEP are presented here.

QCD colour factor

QCD is a gauge theory with SU(3) as underlying gauge group. Eigenvalues of the Casimir operators are called colour factor. A stringent test of QCD would be made from determination of strong coupling constant and the colour factor. The former is the only free parameter of the theory, while the latter tells whether the theory is indeed based on SU(3).

Such measurements have been performed at LEP using 4-jet events, which involve (1) two gluon emission from primary quarks (2) quark-pair splitting from an emitted gluon from a quark, and (3) two gluons from an emitted gluon from a quark (gluon self coupling). Multi-jet rate is also used for the analyses. Recent analyses are based on next-to-leading order perturbative calculations. Figure 13 shows results on the colour factor ratios [14]. They are consistent with the expectation for SU(3) gauge group.

Strong coupling constant and its running

High statistics measurements of strong coupling constant $\alpha_s(m_Z)$ have been performed using Z decays using event shape, hadronic Z width and hadronic decay width of τ leptons. Running of α_s is studied by event shape analyses at LEP2. Hadronic events with hard photon radiation are also used to access the energy below the Z mass. Latest analyses are based on resummed NLLA perturbative QCD calculations for event shape analyses. Combined LEP α_s measurements are shown in figure 13. Recent review of α_s measurements can be found in reference [15].

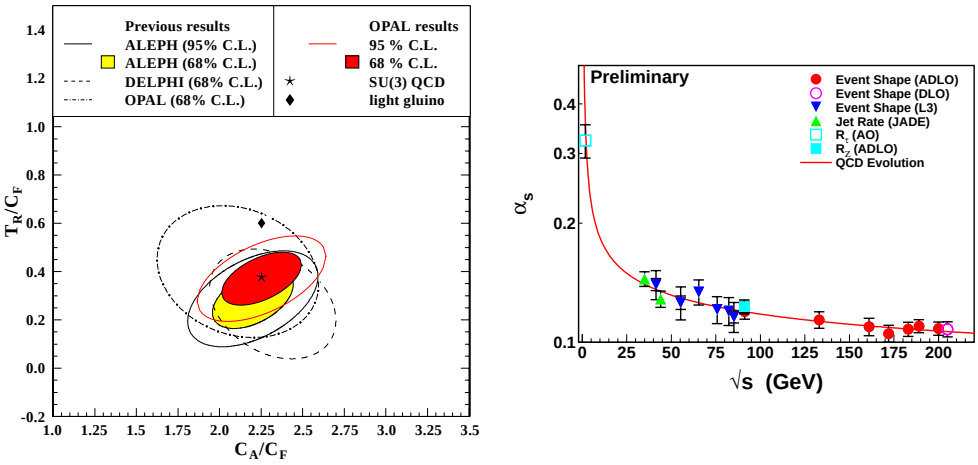

Figure 13: Left: Determination of QCD colour factors. Right: Combined α_s measurements.

4 Measurements above the Z

By the end of LEP-2 operation in 2000, the integrated luminosity collected by each of the LEP experiments, at the centre-of-mass energies above the Z, reached 700 pb^{-1}. The range of centre-of-mass energy is 130 - 209 GeV.

4.1 2-fermion production at LEP2

Studies of fermion pair production have continued at the higher energy of LEP2. At these high energies, fermion pair production may be classified into two kinematic regimes: "radiative events" where the effective collision energy is reduced to the region of Z mass by emitting hard initial-state photons, and "non-radiative" events with collisions at nearly full centre-of-mass energy. Figure 14 shows an example of reconstructed effective centre-of-mass energy, $\sqrt{s'}$, for the process of quark-pair final state. Measured hadronic cross-sections are shown separately for the non-radiative and inclusive events. Measured cross-sections and forward-backward asymmetries

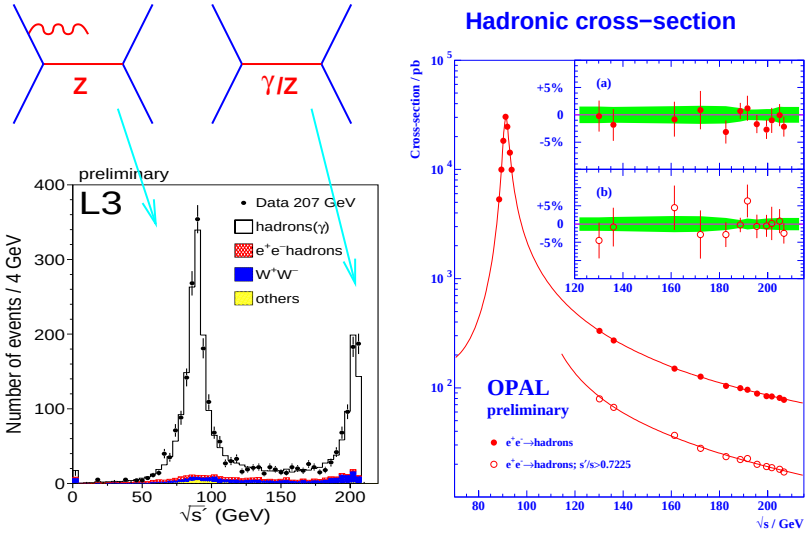

Figure 14: Left: Reconstructed effective centre-of-mass energy $\sqrt{s'}$. Right: Measured hadronic cross-section as a function of centre-of-mass energy, shown separately for inclusive and non-radiative events. The inset shows the ratio to the Standard Model predictions.

for non-radiative events are summarised in figure 15. Similar measurements have been made for electrons, b and c quarks. The Standard Model predictions, obtained using the program ZFITTER agree well with the data.

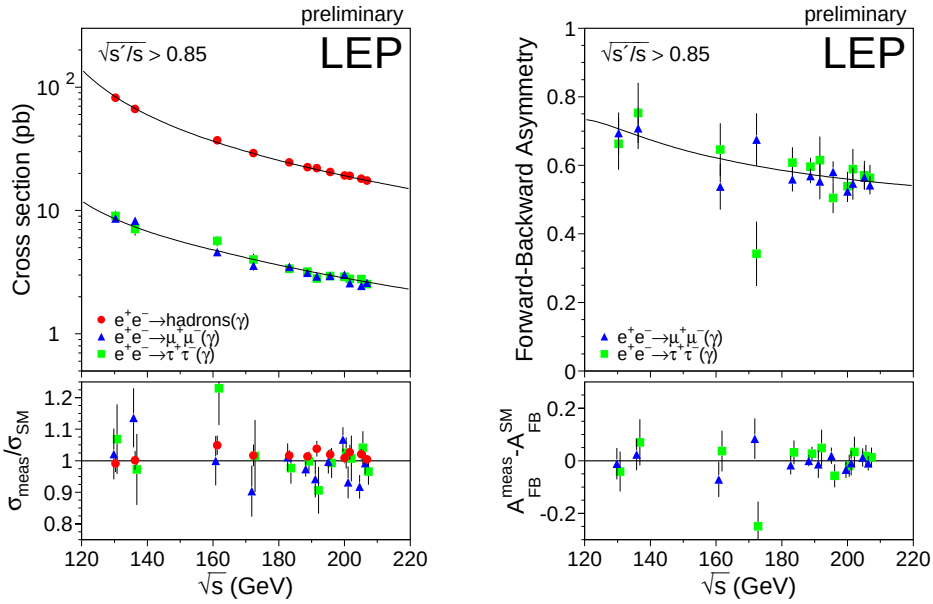

Figure 15: Left: Measured cross-sections for non-radiative hadronic and lepton-pair events. Right: Measured leptonic forward-backward asymmetries for non-radiative events. The curves are predictions of the Standard Model.

Presence of new physics could lead to deviations from the Standard Model predictions. Therefore these measurements have been used to place limits on various new physics possibilities. Some examples are, energy scale of four-fermion contact interaction, mass and mixing angle of additional heavy neutral boson Z′, the energy scale of gravity in models of large extra dimension, mass and coupling of lepto-quarks [12]. Limits are also set on R-parity violating squarks and doubly charged Higgs bosons [16]. Figure 16 shows as an example limits on the energy scale Λ of contact interactions, obtained from the LEP combined cross-sections and forward-backward asymmetries for lepton pair final states.

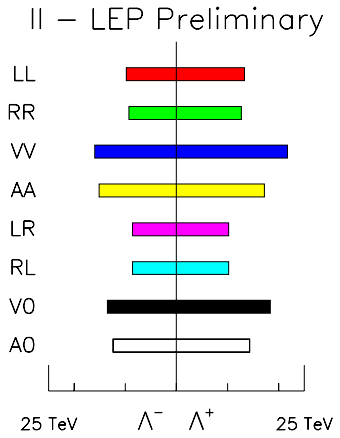

Figure 16: The 95% confidence level limits on the energy scale for different models of contact interaction obtained from analyses of lepton-pair cross-sections and forward-backward asymmetries.

Fermion-pair measurements have also been used for a determination of running electro-

magnetic coupling as a function of energy. At centre-of-mass energies well above the Z mass contribution of s-channel photon exchange is comparable to that from the Z contribution. By parameterising the cross-section and asymmetries as functions of electromagnetic coupling $\alpha(s)$, and assuming all other parameters behave as the Standard Model expectation, electromagnetic coupling is derived from fitting the theoretical predictions to the experimental measurements [17]. Similarly, running coupling $\alpha(t)$ for space-like photon exchange is measured by analysing the process $e^+e^- \to e^+e^-$ where t-channel photon exchange contribution is dominant [18]. Results are depicted in figures 17.

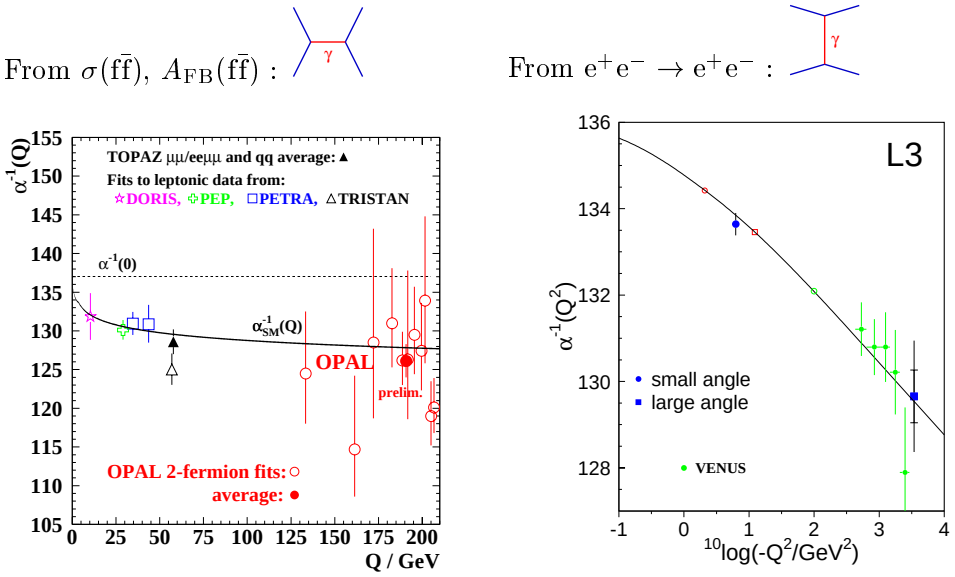

Figure 17: Left: Running α in s-channel. Right: Running α in t-channel. The curves show the Standard Model evolution.

4.2 W physics at LEP2

Each LEP experiments collected about 12,000 W pair events from the full LEP2 data sample at centre-of-mass energy distributed over the range of 161 - 209 GeV. This allows precise measurements of W properties (mass, width and decay branching rates), and direct tests of the unique structure of three gauge boson couplings through systematic studies of production cross-section, angular distribution and W helicity. Detailed discussion on these subjects are found elsewhere [19]. Brief comments on a few topics are given here.

At LEP2, all decay final states from W pair production are identified with good efficiency and purity. W pair cross-section and W decay branching ratios are determined from data without relying much on the Standard Model, allowing direct tests of the Standard Model. Figure 18 shows measured W pair cross-section as a function of centre-of-mass energy. The measured data are compared to the Standard Model expectation obtained using the latest precision calculations. Also shown in the figure are two curves which correspond to two scenarios where one or both of the gauge boson self-couplings were absent. It clearly indicates that there are in fact self-couplings of gauge bosons and the structure of the couplings are as given in the Standard Model. Further detailed studies have been performed which can be found in reference [12, 19].

Mass of the W boson, m_W, is a basic parameter of the nature. In addition, it involves, through the Standard Model relations and radiative corrections, information on other Standard Model parameters. In particular, given the known precise values of $\alpha(m_Z)$, m_Z and G_F, radiative corrections are sensitive to the top mass and yet unknown Higgs mass. Therefore precise determination of m_W allows stringent tests of the Standard Model, and provides information on

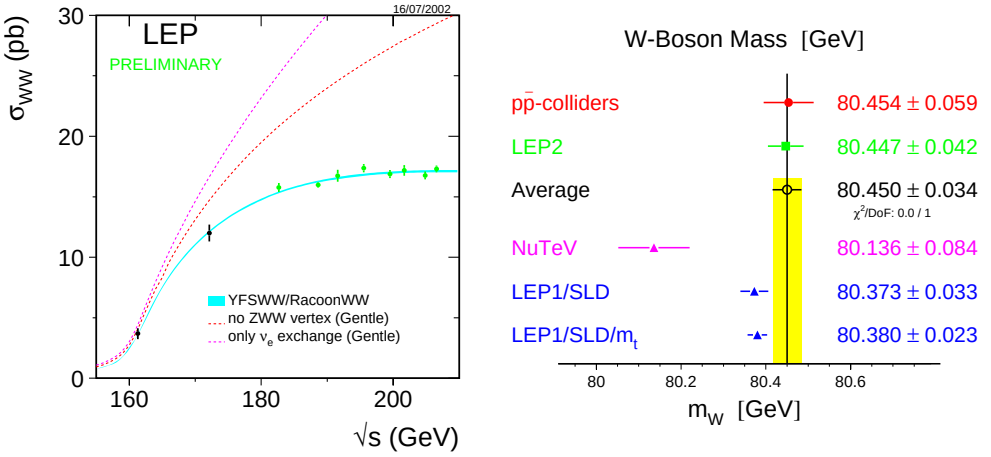

Figure 18: Left: Cross-section for W pair production as a function of centre-of-mass energy. Right: Comparison of W mass measurements.

the Higgs mass. Combined preliminary determination of m_{W} from the results of the four LEP experiments is shown in figure 18. Also shown is the measurement from the $\mathrm{p\bar{p}}$ colliders. These two measurements are based on quite different techniques, and they agree well, yielding an average value of 80.450 ± 0.034 GeV. Accuracy of the LEP measurement is expected to improve further in the final results.

5 Global analysis of the Standard Model

The precision electroweak measurements at LEP and other experiments can be used in the global analysis in the framework of the Standard Model to see whether all data are compatible with the Standard Model expectations for a common set of the Standard Model parameters, and to derive or place constraint on the parameters. Particularly interesting of these parameters is the Higgs mass which is the last unknown Standard Model parameter.

The following data are used in the analysis here [12].

- The Z parameters
  - lineshape and lepton asymmetry at LEP : m_{Z}, Γ_{Z}, σ^0_{had}, R^0_ℓ and $A^{0,\ell}_{\mathrm{FB}}$.
  - Asymmetry parameters $\mathcal{A}_\ell$ from τ polarisation at LEP
  - $\mathcal{A}_\ell$ from polarised left-right asymmetry from SLD
  - Heavy quark measurements at LEP and SLD : R^0_{b}, R^0_{c}, $A^{0,\mathrm{b}}_{\mathrm{FB}}$, $A^{0,\mathrm{c}}_{\mathrm{FB}}$, $\mathcal{A}_{\mathrm{b}}$ and $\mathcal{A}_{\mathrm{c}}$
  - $\sin^2\theta^{\mathrm{lept}}_{\mathrm{eff}}$ from inclusive quark forward-backward asymmetry at LEP
- W mass m_{W} and width Γ_{W} from LEP and Tevatron $\mathrm{p\bar{p}}$ collider
- Top mass m_{t} at Tevatron [20]
- Light quark contribution to the running of α : $\Delta\alpha^{(5)}_{\mathrm{h}}(m_{\mathrm{Z}})$ [4]
- $\sin^2\theta_{\mathrm{W}} = 1 - m^2_{\mathrm{W}}/m^2_{\mathrm{Z}}$ from νN scattering data by the NuTeV experiment [21]
- Weak charge Q_W from the atomic parity violation for Cs.

The values of these inputs are summarised in figure 21.

Standard Model predictions of these observables depend on a few parameters. The set of parameters chosen are: $\alpha(m_{\rm Z})$, $m_{\rm Z}$ and G_F as the three basic parameters of the electroweak interaction, and $\alpha_s(m_{\rm Z})$ for QCD. In addition top mass $m_{\rm t}$ and Higgs mass $m_{\rm H}$ are needed to calculate radiative corrections. The latest version of ZFITTER and TOPAZ0 programs are used. Apart from the the precisely known G_F, there remain five relevant parameters:

$$m_{\rm Z},\ m_{\rm t},\ m_{\rm H},\ \alpha_s(m_{\rm Z}),\ \Delta\alpha^{(5)}_{\rm h}(m_{\rm Z})\ . \tag{43}$$

Some of the measurements in the list can be used to directly constrain these parameters ($m_{\rm Z}$, $\Delta\alpha^{(5)}_{\rm h}(m_{\rm Z})$, $m_{\rm t}$), while other observables are calculated in the Standard Model and compared to the experimental results.

As seen in section 2 effects of electroweak radiative correction appear in $\Delta\rho$ and $\Delta\kappa$ (thus $\sin^2\theta^{\rm f}_{\rm eff}$). They control the size of Z partial widths $\Gamma_{\rm f}$ and asymmetry parameters $\mathcal{A}_{\rm f}$. In case of the hadronic width $\Gamma_{\rm had}$, QCD final state correction is also included, therefore it is sensitive to the strong coupling constant $\alpha_s(m_{\rm Z})$. There are additional corrections to the b quark couplings arising from the vertex correction, leading to unique dependence of $\Gamma_{\rm b}$ on $m_{\rm t}$. Finally the W mass contains the correction Δr

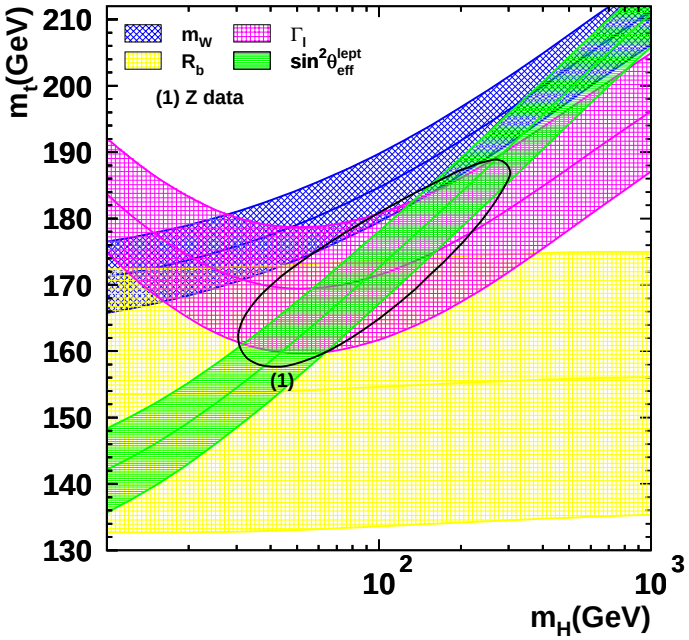

Figure 19: The bands show the regions corresponding to the one standard deviation ranges of the measurements of $m_{\rm W}$, Γ_ℓ, $R^0_{\rm b}$ and $\sin^2\theta^{\rm lept}_{\rm eff}$. The contour shows the 68% probability area determined from a global fit to the Z data.

The observables from LEP/SLD measurements are combination of these quantities: $m_{\rm Z}$, $\Gamma_{\rm f}$, $\sin^2\theta^{\rm f}_{\rm eff}$, and $m_{\rm W}$. Depending on how the observables are constructed from these quantities, the sensitivity to the Standard Model parameters are different. For example, asymmetry measurements determine $\mathcal{A}_{\rm f}$, which is sensitive to $m_{\rm t}$ and $m_{\rm H}$. On the other hand partial width ratio $R^0_\ell = \Gamma_{\rm had}/\Gamma_\ell$ is insensitive to $m_{\rm t}$ and $m_{\rm H}$ due to large cancellation of universal corrections included in both of $\Gamma_{\rm had}$ and Γ_ℓ, but it is sensitive to the strong coupling constant which is involved in the QCD correction on $\Gamma_{\rm had}$. The hadronic pole cross-section $\sigma^0_{\rm had} = (12\pi/m^2_{\rm Z})\Gamma_{\rm e}\Gamma_{\rm had}/\Gamma^2_{\rm Z}$ has only weak sensitivity to any of the Standard Model parameters. This is because in addition to

the cancellation of universal corrections in the Z widths, the QCD correction, which is included both in $\Gamma_{\rm had}$ and $\Gamma_{\rm Z}$, also cancels largely. However, $\sigma^0_{\rm had}$ is sensitive to the invisible width, or, number of neutrinos N_ν which directly determine the total width $\Gamma_{\rm Z}$.

R^0_ℓ is one of the sensitive parameter to the QCD couping constant $\alpha_s(m_{\rm Z})$. For $m_{\rm Z} = 91.1875 \pm 0.0021$ GeV and $m_{\rm t} = 174.3 \pm 5.1$ GeV, $\alpha_s(m_{\rm Z}) = 0.1224 \pm 0.0038$ is obtained. Alternatively, from the leptonic pole cross-section σ^0_ℓ, $\alpha_s(m_{\rm Z}) = 0.1180 \pm 0.0030$ is derived. These are in good agreement with the world averages [15, 20].

To see how these observables place constraints on $m_{\rm t}$ and $m_{\rm H}$ through radiative corrections, figure 19 shows in the $m_{\rm H}$ - $m_{\rm t}$ plane the constraints set by the measurements of four sensitive observables: Γ_ℓ, $\sin^2\theta^{\rm lept}_{\rm eff}$, $R^0_{\rm b} = \Gamma_{\rm b}/\Gamma_{\rm had}$ and $m_{\rm W}$. Note that $R^0_{\rm b}$ is insensitive to $m_{\rm H}$ and provide constraint on $m_{\rm t}$ almost independently of $m_{\rm H}$. The contour shows the 68% confidence level region determined from the Z data only, without using $m_{\rm W}$ and $m_{\rm t}$. This can be compared to the constraint from $m_{\rm W}$. They are reasonably consistent each other.

As an another way of presentation, figure 20 shows in the $m_{\rm t}$ - $m_{\rm W}$ plane the constraint using indirect measurements only, and comparison with the direct measurements. Direct and

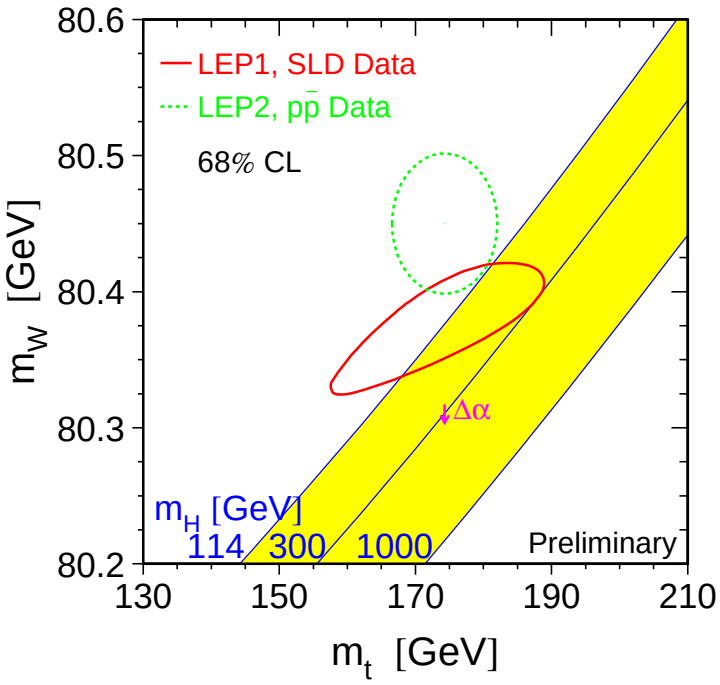

Figure 20: The comparison of the indirect measurements of $m_{\rm W}$ and $m_{\rm t}$ and the direct measurements. In both cases the 68% probability contours are shown. Also shown is the Standard Model relation between two masses for given values of $m_{\rm H}$.

indirect determinations are consistent each other, an important test of the Standard Model at the level of radiative corrections. W mass obtained from the indirect determination is shown in figure 18 and compared to the direct determination. Also shown in the figure 20 are trajectories corresponding to given values of Higgs mass $m_{\rm H}$. Comparison of these lines and confidence contours indicates that the data are sensitive to the Higgs mass, and the data prefer low $m_{\rm H}$.

The best constraint on the Higgs mass is obtained by using all data including $m_{\rm W}$ and $m_{\rm t}$. Figure 21 shows $\Delta\chi^2 = \chi^2 - \chi^2_{min}$ of the fit as a function of $m_{\rm H}$, and the pull of each observable. The χ^2/d.o.f is 29.7/15 which corresponds to the probability of 1.3%. Higgs mass at the minimum χ^2 is 81 GeV. The 95% upper bound on $m_{\rm H}$, including theoretical uncertainties, is 193 GeV, while the lower bound on $m_{\rm H}$ obtained from the direct searches at LEP is 114.4 GeV at the 95% confidence level [22].

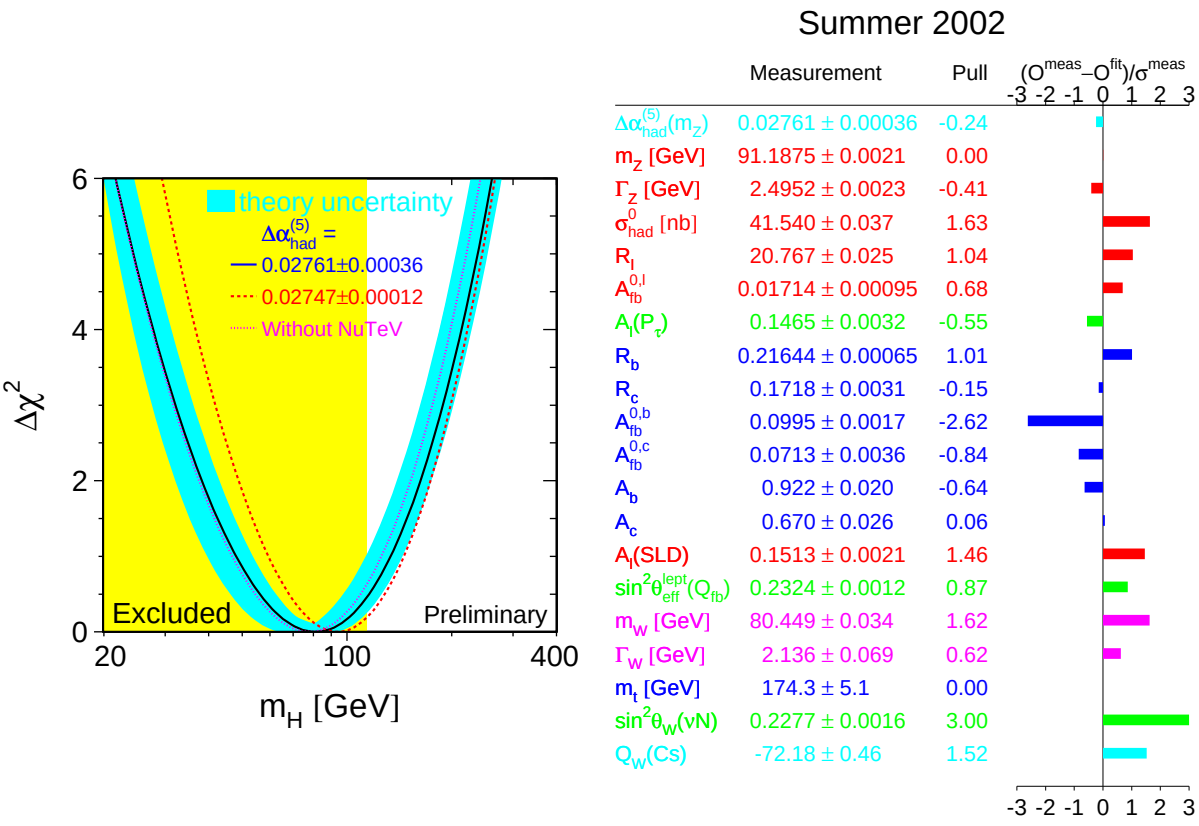

Figure 21: Left: $\Delta\chi^2$ as a function of $m_{\rm H}$ using all data. Right: Pull of each input data in the global fit.

The poor χ^2 is partly due to the disagreement between $\mathcal{A}_\ell$ and $A_{\rm FB}^{0,\rm b}$. In addition a large contribution is due to the $\sin^2\theta_{\rm W}$ from the NuTeV result which contribute 9 units to χ^2. The NuTeV $\sin^2\theta_{\rm W}$ can be converted to $m_{\rm W}$ and compared to the direct determination of $m_{\rm W}$ (figure 18). Agreement is marginal. Removing the NuTeV result from the global fit causes little change on the fitted $m_{\rm H}$, but the overall χ^2 reduces to 20.5/14 (probability 11%).

6 Unrealised LEP programs

Before closing the report, brief remarks are made here about ideas for further upgrading the physics potential of LEP, once studied, proposed, but not realised.

6.1 Polarisation at LEP

Longitudinal polarisation of LEP would allow precise measurement of $\sin^2\theta_{\rm eff}^{\rm lept}$ from A_{LR} at LEP. Such measurement has been made only at the SLC linear collider. Importance of longitudinally polarised beam was recognised already in early time, and a workshop on polarisation at LEP was held in 1987. At LEP, transverse polarisation of electrons, along the direction of bending dipole field, occurs naturally, if conditions are met to avoid depolarising effects, by the Sokolov-Ternov effect by emitting synchrotron radiation. Spin direction is opposite for electrons and positrons. Then vertical spin direction must be rotated to longitudinal direction at the entrance to the straight section where the detector is located, and rotated back to vertical when leaving the intersection point so that the polarisation is maintained in the arc. Such spin rotator can

be realised by a pair of dipole magnets with magnetic field in horizontal direction. If all the electron and positron bunches are polarised, the consequence is not very interesting, because it leads to the spin configuration where the Z cross-section vanishes: figure 22(a). However by selectively depolarising particular bunches, this problem is avoided, and furthermore it allows self calibration of various systematics: figure 22(b).

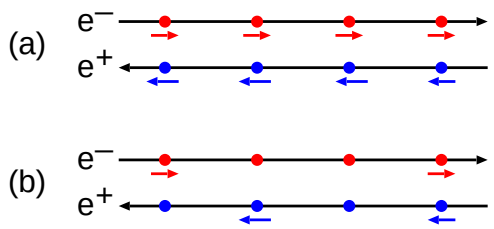

Figure 22: Configuration of longitudinal spin polarisation at LEP. (a) all four bunches are polarised. (b) selectively depolarising particular bunches.

Four different spin configurations appear which correspond to:

$$e^-_R e^+,\ e^- e^+_R,\ e^- e^+,\ e^-_R e^+_R \tag{44}$$

The first two combinations provide a measurement of left-right asymmetry of Z cross-section. The third combination gives unpolarised cross-section, while the cross-section for the forth combination is zero if e^- and e^+ are 100% polarised. If the degree of polarisation is P, observed left-right asymmetry is scaled by this factor: $A_{LR}(obs) = P \cdot A_{LR}$. Cross-section for the fourth combination is $(1 - P^2)$ of unpolarised cross-section, therefore it provides a handle to monitor the beam polarisation.

Idea of polarised LEP was pursued and a proposal was made in 1995 to make a test of longitudinal polarisation. The project included, building a test spin rotator making use of existing dipole magnets, and constructing a simple detector which can identify hadronic Z decays and precision luminosity measurements, so that a measurement of A_{LR} could be made. Machine studies were made to see for example the feasibility of maintaining polarisation with colliding beams. Due to various difficulties, eg. conflict with the LEP2 energy upgrade program, technical uncertainties, the project has never been realised, though it was recognised as a worthwhile option after LEP2.

Transverse beam polarisation was however used as a crucial element of the precise beam energy calibration.

6.2 High luminosity LEP

Another radical idea [24] of possible LEP upgrade was to increase LEP luminosity significantly, aiming for 10^7 Z, in order to improve the precision of statistically limited measurements(B oscillation, asymmetry measurements,...), and also to gain sensitivity to possible new physics which may appear as rare events. The method considered was to increase the number of bunches, from the original four bunches per beam to up to 36 bunches. This could be realised by using a special 'pretzel' orbit in order to avoid bunch collisions in the arc. Experiments have studied feasibility of running under condition of large number of bunches, and concluded that more than 8 bunches would require substantial modifications. These studies lead to the LEP operation in 1993 and 1994 with 8-bunch pretzel orbit. It should be noted that many of the anticipated physics potential with 'high luminosity' LEP was actually realised, from efficient running of LEP at the Z pole until 1995, very good performance of micro-vertex detectors and careful combination of results from the four LEP experiments.

7 Conclusion

The twelve years of data-taking by the LEP experiments have made big contribution to establish the Standard Model. Precision results from LEP, and other experiments, allowed to test the Standard Model to the level of radiative correction, and it seems the Standard Model is well established. Agreement between indirect and direct determinations of m_{W} and m_{t} is a demonstration of such tests. Similar analysis has been repeated to predict the Higgs mass. Current knowledge on the probably Higgs mass is in the range of 114.4 - 193 GeV as inferred from the results of direct searches and indirect bound through the analysis of precision measurements in the framework of the Standard Model.

Analysis work is still continuing for both LEP1 and LEP2 data. Improvements can still be expected in the W mass measurement, from better understanding of final-state hadronic interaction effects for example.

There are a few measurements showing two to three standard deviation differences, for example the measurements of $A_{\mathrm{FB}}^{0,\mathrm{b}}$ and $\mathcal{A}_\ell$, which may be simple fluctuations or might be an indication of some new physics. Further improvements of experimental data will come slowly in future: by completing and finalising the remaining LEP analyses, and new information from the current and future experiments, including new set of m_{W} and m_{t} measurements from Tevatron which has recently restarted running. LHC will further contribute to these precision measurements, and more essentially discovery and studies of the nature of the Higgs boson. Future $\mathrm{e^+e^-}$ linear collider will follow to make a new round of precision and systematic survey of physics, hopefully be including new physics beyond the current Standard Model.

References

1. R. Tanaka, in these proceedings.
2. `http://alephwww.cern.ch/WWW/`
   `http://delphi.web.cern.ch/Delphi/Welcome.html`
   `http://l3www.cern.ch/`
   `http://opal.web.cern.ch/Opal/`
3. The BES collaboration,J.Z. Bai *et al.*, *Phys. Rev. Lett.* **88**, 101802 (2002).
4. H. Burkhardt and B. Pietrzyk, *Phys. Lett.* B **513**, 46 (2001)
5. SLD collaboration, K. Abe *et al.*, *Phys. Rev. Lett.* **84**, 5945 (2000).
6. The LEP energy working group, R. Assmann *et al.*, *Eur. Phys. J.* C **6**, 187 (1999).
7. D. Bardin *et al.*, *Z. Phys.* C **44**, 493 (1989); *Comp. Phys. Comm.* **59**, 303 (1990); *Nucl. Phys.* B **351**, 1 (1991); *Phys. Lett.* B **255**, 290 (1991) and CERN-TH 6443/92(May 1992); DESY 99-070, hep-ph/9908433 (Aug 1999); *Comp. Phys. Comm.* **133**, 220 (2001).
8. G. Montagna *et al.*, *Comp. Phys. Comm.* **76**, 329 (1993).
9. D. Bardin, M. Grunewald and G. Passarino, 'Precision calculation project report', hep-ph/9902452.
10. LEP collaborations and the LEP electroweak working group, "Combination procedure for the precise determination of Z boson parameters from results of the LEP experiments", CERN-EP-2000-153, hep-ex/0101027.
11. The LEP collaborations, the LEP electroweak working group and the SLD heavy flavour and electroweak groups, "A combination of preliminary electroweak measurements and constraints on the Standard Model", CERN-EP-2001-98, hep-ex/0112021
12. The LEP electroweak working group, results prepared for 2002 summer conferences. To be published in CERN-EP preprint; http://lepewwg.web.cern.ch/LEPEWWG/
13. S. Bethke, "Eleven years of QCD at LEP", hep-ex/0112032, *Eur. Phys. J. direct* C 4, 1 (2002).

14. OPAL collaboration, G. Abbiendi *et al.*, *Eur. Phys. J.* C **20**, 601 (2001).
15. S. Bethke, "Determinations of the QCD coupling α_s", MPI-PhE 2000-07, hep-ex/0004021.
16. The OPAL collaboration, OPAL physics note PN502 (July 2002).
17. OPAL collaboration, G. Abbiendi *et al.*, *Eur. Phys. J.* C **13**, 553 (2000); OPAL Physics note PN437 (July 2000).
18. L3 collaboration, M. Acciarri *et al.*, *Phys. Lett.* B **476**, 40 (2000).
19. T. Saeki, in these proceedings.
20. Particle Data Group, D.E. Groom *et al.*, *Eur. Phys. J.* C **15**, 1 (2000).
21. NuTeV collaboration, G.P. Zeller *et al.*, *Phys. Rev. Lett.* **88**, 091802 (2002).
22. T. Mori, in these proceedings;
23. "Polarization at LEP", CERN-88-06 1988
24. "Report of the working group on high luminosities at LEP", CERN-91-02 1991